Quantitative microCT imaging of a whole equine placenta and its blood vessel network

Davis Laundon, Ella Proudley, Philip J Basford, Orestis L Katsamenis, David S Chatelet, Jane K Cleal, Neil J Gostling, Pascale Chavatte-Palmer, Rohan M Lewis

HAL Id: hal-04678493
https://hal.inrae.fr/hal-04678493v1

Submitted on 27 Aug 2024

Quantitative microCT imaging of a whole equine placenta and its blood vessel network

Davis Laundon [a,b,*], Ella Proudley [a], Philip J. Basford [b,c,d], Orestis L. Katsamenis [b,d], David S. Chatelet [e], Jane K. Cleal [a,b], Neil J. Gostling [b,f], Pascale Chavatte-Palmer [g,h], Rohan M. Lewis [a,b]

[a] *The Institute of Developmental Sciences, Human Development and Health, Faculty of Medicine, University of Southampton, Southampton, SO16 6YD, UK*
[b] *Institute for Life Sciences, University of Southampton, University Rd, Highfield, Southampton, SO17 1BJ, UK*
[c] *School of Engineering, Faculty of Engineering and Physical Sciences, University of Southampton, University Road, Southampton, SO17 1BJ, UK*
[d] *μ-VIS X-Ray Imaging Centre, Faculty of Engineering and Physical Sciences, University of Southampton, Southampton, SO17 1BJ, UK*
[e] *Biomedical Imaging Unit, Faculty of Medicine, University of Southampton, Southampton, SO16 6YD, UK*
[f] *School of Biological Sciences, Faculty of Environmental and Life Sciences, University of Southampton, University Rd, Highfield, Southampton, SO17 1BJ, UK*
[g] *Université Paris-Saclay, UVSQ, INRAE, BREED, 78350, Jouy-en-Josas, France*
[h] *Ecole Nationale Vétérinaire d'Alfort, BREED, 94700, Maisons-Alfort, France*

A R T I C L E   I N F O

A B S T R A C T

Placental structure is linked to function across morphological scales. In the placenta, changes to gross anatomy, such as surface area, volume, or blood vessel arrangement, are associated with suboptimal physiological outcomes. However, quantifying each of these metrics requires different laborious semi-quantitative methods. Here, we demonstrate how, with minimal sample preparation, whole-organ computed microtomography (microCT) can be used to calculate gross morphometry of the equine placenta and a range of additional metrics, including branching morphometry of placental vasculature, non-destructively from a single dataset. Our approach can be applied to quantify the gross structure of any large mammalian placenta.

1. Introduction

Placental morphometry is linked to physiological outcomes [1]. The mammalian placenta exhibits remarkable morphological diversity across structural scales [2–4], the largest of which is 'gross morphology' [4]. Gross morphology refers to macroscopic structural characterisation of the placenta at the whole-organ level. Changes to gross placental morphology are associated with suboptimal gestational outcomes [5], such as intrauterine growth retardation [6,7]. Horses exhibit a diffuse placenta, whereby a villous allantochorion covers the entire endometrial surface for nutrient exchange with the mother [8–10]. Different metrics for quantifying equine placentas must currently be measured using different methodologies. For instance, gross surface area is measured by placing the placenta beneath a clear acrylic sheet marked with gridlines, while gross volume is determined through water displacement [8,11]. Blood vessel architecture, which is important for understanding blood flow and nutrient transport, is often assessed via corrosion casting, a

technique involving resin injection into the vessels followed by tissue removal [12–14]. Such methodologies are less precise than modern approaches, and some of them are time-consuming, destructive, and labour-intensive. Three-dimensional (3D) imaging techniques can quantify placental tissue architecture and reveal structures not apparent in two-dimensions [4,15]. Of these, microCT (or X-ray microfocus Computed Tomography) has emerged as a powerful non-destructive tool to quantify tissue architecture at the level of both the whole placenta [16,17] and microanatomy [4,18]. Here, we demonstrate how microCT can be used to quantify the gross morphometry of the equine placenta. Although we focus on the equine placenta for its veterinary and comparative implications, our approach is applicable to quantifying the structure of any large mammalian placenta.

2. Methods

We scanned an entire equine placenta (New Forest Pony, *Equus*

---

caballus) using microCT (Fig. 1). Following collection, the placenta was washed in 1 x PBS, fixed in 10 % buffered formalin, and immersed in 10 % Lugol's iodine solution (Fig. 1A–C) prior to imaging in a walk-in microCT system (diondo d5; Fig. 1D–F). The resulting volume image dataset (Fig. 1G and H) was segmented (Fig. 1I), 3D reconstructed, and quantified within Microscopy Image Browser (MIB) [19] as in Ref. [20]. The full methodology is available in the *Supplementary Methods*. The full image dataset and corresponding labels are freely available for download at Bioimage Archive accession S-BIAD1130 under license CC BY 4.0 https://www.ebi.ac.uk/biostudies/bioimages/studies/S-BIAD1130. Analysis of samples in Southampton was approved locally by the University of Southampton (47770.A1/46381.A2).

3. Results and discussion

With only minimal and reversable sample preparation [21], we quantified the surface area of the allantochorion, volume of major components, and branching morphometry of major blood vessels in a whole equine placenta using this single technique. Whole-organ microCT imaging of the entire equine placenta permitted quantitative morphometric analysis (Fig. 2; Video 1). The allantochorionic placenta had a total volume of 1411 cm^3 and an outer chorionic surface area of 9126 cm^2 (inner surface of 7561 cm^2) (Fig. 2A). The amniotic sac,

umbilical cord, blood vessels (ranging from ~0.2–1.2 cm in diameter) and allantoic pouches were also reconstructed (Fig. 2B–D) and volumetrically quantified (Fig. 2E). Allantoic pouches ranged from 13 to 470 mm^3 in volume (mean ± SD, 146 ± 144 mm^3) and we can visualise their distribution around the umbilical cord attachment site (Fig. 2D). The reconstructed blood vessels could be traced and quantified for branching metrics (Fig. 2F–K), which is not possible using semi-quantitative 2D techniques. Due to the 3D connectivity of the microCT dataset, individual vessels could be traced and separated, delineating arterial and venous vessels (Fig. 2F). The two umbilical arteries could be further separated, resolving the three major umbilical vessels and their trajectories (Fig. 2G). This showed that one artery localises to the pregnant horn and placental body, whereas the other localises to the non-pregnant horn (Fig. 2G). Skeletonised vessels were then quantified morphometrically (Fig. 2H–K), showing that the artery in the non-pregnant horn was notably shorter, less branched, and had a lower branching angle than either the artery in the pregnant horn or the vein (Fig. 2J and K). We can also see that the vein covers a much larger area of the placenta (as quantified by 'Convex Volume') than either artery individually (Fig. 2K). The distribution of these data can be visualised graphically (Fig. 2J) and could be statistically compared between treatments.

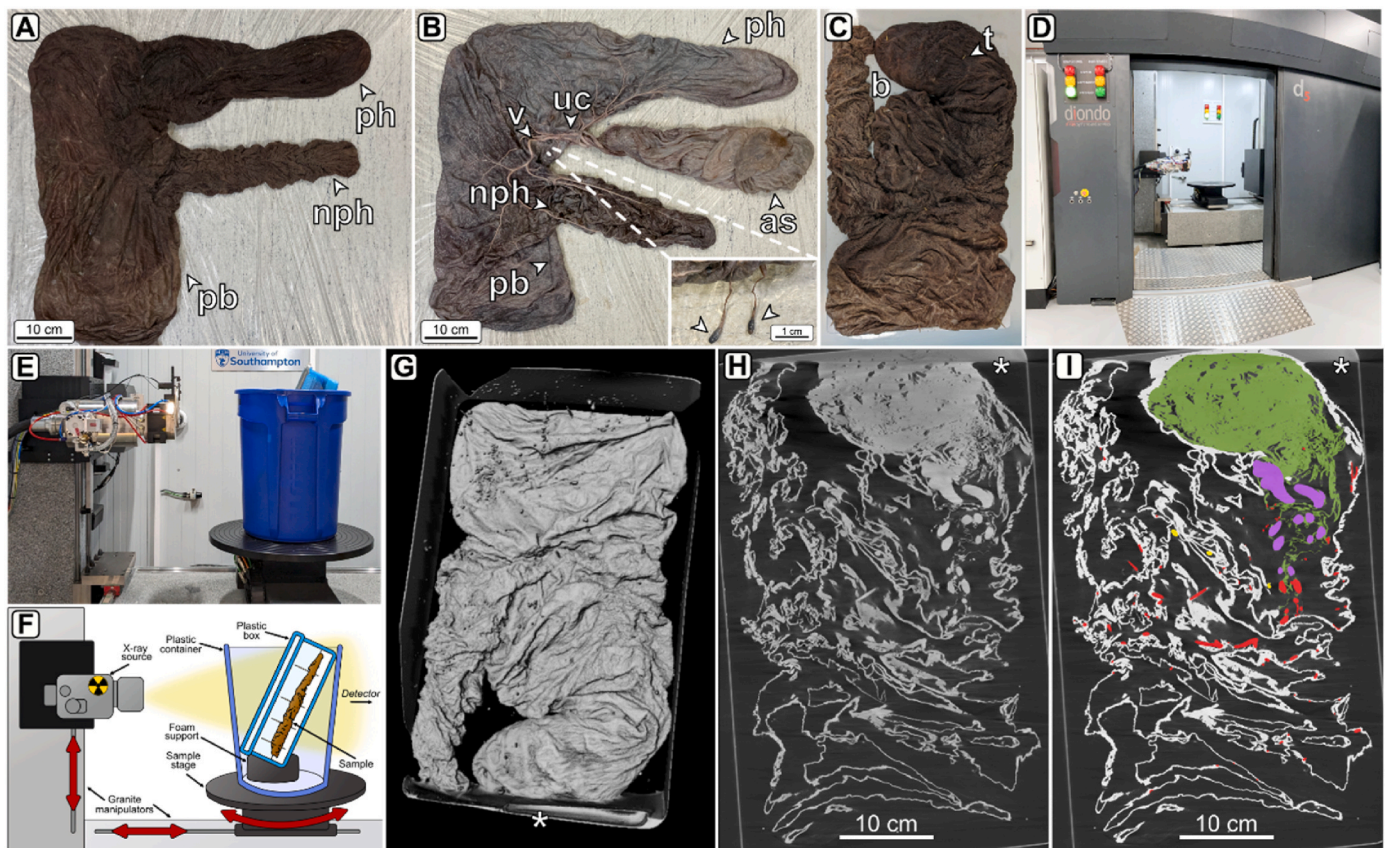Our whole-organ microCT imaging of the equine placenta achieved a

Fig. 1. – **Whole-organ microCT imaging of an entire equine placenta**. (A–B) Photographs of the fixed and stained New Forest Pony (*Equus caballus*) placenta used in this study arranged in the classic 'F' configuration, shown with the chorionic surface facing both out (**A**) and in (**B**). Labelled are the amniotic sac (as), the placental body (pb), the pregnant horn (ph), the non-pregnant horn (nph), the umbilical cord (uc), and major vessels (v). Inset in B shows examples of allantoic pouches typically found around the umbilical cord attachment site. (**C**) Prior to scanning, the placenta was adhered to a polystyrene board (b) with wooden toothpicks (t). The amniotic sac and umbilical cord were inserted inside the internal cavity of the pregnant horn, and the placenta imaged chorionic side out. (**D**) Exterior of the diondo d5 walk-in microCT system used in this study, located at the μ-VIS X-ray Imaging Centre (www.muvis.org) at the University of Southampton, UK. (**E-F**) Photographic (E) and diagrammatic (F) representation of the scanning setup inside the d5 system used in this study. A plastic container was used to capture any liquid leaks and prevent damage to the equipment. (**G**) Volumetric render of the microCT dataset illustrating the approximate orientation of the placenta during scanning. A small pool of fluid accumulated at the bottom of the box (asterisk). (**H-I**) Virtual slice through the microCT dataset (H) and corresponding label segmentation (I) of the imaged equine placenta. Labelled are the allantoic pouches (yellow), amniotic sac (green), umbilical cord (purple) and non-umbilical blood vessels (red). The orientation of the sample is as in (C), such that the pool of fluid is now located at the top of the image (asterisk).
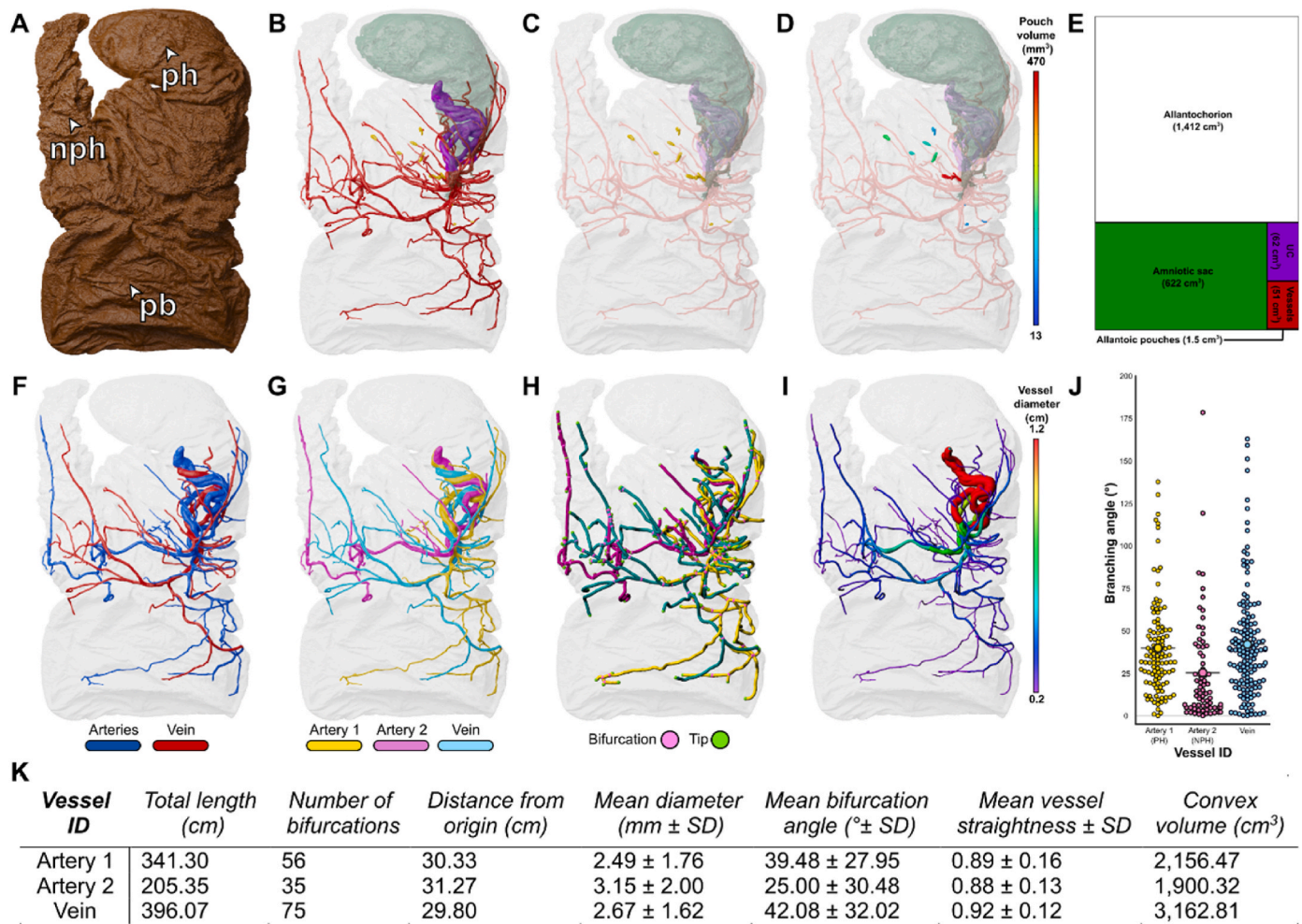
Vessel ID	Total length (cm)	Number of bifurcations	Distance from origin (cm)	Mean diameter (mm ± SD)	Mean bifurcation angle (° ± SD)	Mean vessel straightness ± SD	Convex volume (cm³)
Artery 1	341.30	56	30.33	2.49 ± 1.76	39.48 ± 27.95	0.89 ± 0.16	2,156.47
Artery 2	205.35	35	31.27	3.15 ± 2.00	25.00 ± 30.48	0.88 ± 0.13	1,900.32
Vein	396.07	75	29.80	2.67 ± 1.62	42.08 ± 32.02	0.92 ± 0.12	3,162.81

Fig. 2. – Quantification of equine placental morphometry by whole-organ microCT. (**A**) 3D pseudocoloured reconstruction of the chorionic surface of the scanned equine placenta. Labelled are the placental body (pb), pregnant horn (ph), and nonpregnant horn (nph). (**B**) Internal components of the imaged placenta. Labelled are the allantoic pouches (yellow), amniotic sac (green), umbilical cord (purple) and non-umbilical blood vessels (red). The allantochorion is shown in low-opacity for context (white). (**C-D**) Allantoic pouches (C) were identified around the umbilical cord insertion site and coloured by volume (D). (**E**) Volumetric quantification of labelled structures in the equine placenta. (**F-K**) Filament tracing, visualisation, and quantification of vessel morphometrics of individual vessels from the equine placenta. (F–G) Vessels coloured as arterial or venous in flow (F) and as individual vessels (G). (H–I) Traced vessels showing branching bifurcations and tips (H) and coloured by vessel diameter (I). (J) Distribution of individual branching angles for individual vessel branches (single points). Large circles represent mean values per vessel. (K) Comparison of major vessel morphometrics for the three labelled individual vessels.

holistic quantification of its anatomy using diverse morphometric parameters, all with a single non-disruptive technique, accommodating subsequent analysis including classical histology. As microCT images tissue ridges and folds in 3D, it is not necessary to stretch the placenta into a 2D approximation to get an accurate surface area quantification, as in traditional methods. It should be noted that our data provide only the calculation of gross anatomy and quantification of finer surface structures, such as chorionic villi and capillaries, would require additional higher resolution imaging techniques. This could involve sampling small ~0.5 cm subregions of the chorionic surface prior to microCT imaging for downstream correlative microCT-volume electron microscopy (CXEM) or 3D X-ray histology using higher resolution microCT scanners [22] and other modalities to generate multiscale structural data, as we have described previously [4,18,20]. Segmentation of the microCT datasets can also be a limitation to this methodology, as labelling structures in serial 2D is time-consuming, however segmentation using AI [23] can speed up this process and has shown to be useful in segmenting placental microCT datasets [17].

Here, we demonstrate the application of whole-organ microCT imaging as a powerful tool for quantifying gross placental morphometry. Our central approach of sample preparation and image reconstruction

can also be translated to imaging placentas with more widely available MRI or CT scanners in medical or veterinary settings. As such, we are confident the scope of our workflow can be widely applied. Reconstructed placentas using this technique can be used to investigate changes in gross morphometry in cases of pathology, in interspecies evolutionary comparisons, and as 3D architectures in which to computationally model physiological processes. We therefore propose whole-organ microCT as a tool with great potential to shed light on placental structure and function.

Funding

CRediT authorship contribution statement

Davis Laundon: Writing – review & editing, Writing – original draft, Visualization, Validation, Resources, Project administration, Methodology, Investigation, Formal analysis, Data curation, Conceptualization. **Ella Proudley:** Writing – review & editing, Methodology, Investigation.

Philip J. Basford: Writing – review & editing, Software, Methodology, Formal analysis, Data curation. **Orestis L. Katsamenis:** Writing – review & editing, Software, Methodology, Investigation, Formal analysis, Data curation. **David S. Chatelet:** Writing – review & editing, Software, Methodology, Formal analysis, Data curation. **Jane K. Cleal:** Writing – review & editing, Resources. **Neil J. Gostling:** Writing – review & editing, Supervision, Project administration, Funding acquisition. **Pascale Chavatte-Palmer:** Writing – review & editing, Supervision, Project administration, Funding acquisition. **Rohan M. Lewis:** Writing – review & editing, Writing – original draft, Validation, Supervision, Project administration, Investigation, Funding acquisition, Formal analysis, Conceptualization.

Declaration of competing interest

We declare we have no competing interests.

Acknowledgements

Appendix A. Supplementary data

Supplementary data to this article can be found online at https://doi.org/10.1016/j.placenta.2024.07.313.

References

[1] A.L. Fowden, A.J. Forhead, P.M. Coan, G.J. Burton, The placenta and intrauterine programming, J. Neuroendocrinol. 20 (4) (2008) 439–450.

[2] R. Leiser, P. Kaufmann, Placental structure - in a comparative aspect, Exp. Clin. Endocrinol. 102 (3) (1994) 122–134.

[3] S. Furukawa, Y. Kuroda, A. Sugiyama, A comparison of the histological structure of the placenta in experimental animals, J. Toxicol. Pathol. 27 (1) (2014) 11–18.

[4] D. Laundon, N.J. Gostling, B.G. Sengers, P. Chavatte-Palmer, R.M. Lewis, Placental evolution from a three-dimensional and multiscale structural perspective, Evolution 78 (2023) 13–25.

[5] T. Chenier, The importance of thorough evaluation of the fetal membranes of the mare, Equine Vet. Educ. 23 (2011) 119–120.

[6] S. Biswas, S.K. Ghosh, Gross morphological changes of placentas associated with intrauterine growth restriction of fetuses: a case control study, Early Hum. Dev. 84 (6) (2008) 357–362.

[7] M. Robles, P.M. Peugnet, S.A. Valentino, C. Dubois, M. Dahirel, M.C. Aubrière, F. Reigner, D. Serteyn, L. Wimel, A. Couturier-Tarrade, P. Chavatte-Palmer, Placental alterations in structure and function in intra-uterine growth-retarded horses, Equine Vet. J. 50 (3) (2018) 405–414.

[8] W.R. Allen, S. Wilsher, C. Turnbull, F. Stewart, J. Ousey, P.D. Rossdale, A. L. Fowden, Influence of maternal size on placental, fetal and postnatal growth in the horse. I. Development in utero, Reproduction 123 (3) (2002) 445–453.

[9] P. Chavatte-Palmer, E. Derisoud, M. Robles, Pregnancy and placental development in horses: an update, Domest. Anim. Endocrinol. 79 (2022).

[10] M. Pozor, Equine placenta–A clinician's perspective. Part 1: normal placenta–Physiology and evaluation, Equine Vet. Educ. 28 (2016) 327–334.

[11] M.C. Veronesi, M. Villani, S. Wilsher, A. Contri, A. Carluccio, A comparative stereological study of the term placenta in the donkey, pony and Thoroughbred, Theriogenology 74 (4) (2010) 627–631.

[12] R. Leiser, C. Pfarrer, M. Abd-Elnaeim, V. Dantzer, Feto-maternal anchorage in epitheliochorial and endotheliochorial placental types studied by histology and microvascular corrosion casts, Placenta 19 (1998) 21–39.

[13] A. Saber, M. Abd-Elnaeim, T. Hembes, C. Pfarrer, A. Salim, R. Leiser, Light and scanning electron microscopic study on the blood vascular system of the donkey placenta, Anat. Histol. Embryol. 37 (2) (2008) 86–94.

[14] T.O. Junaid, R.S. Bradley, R.M. Lewis, J.D. Aplin, E.D. Johnstone, Whole organ vascular casting and microCT examination of the human placental vascular tree reveals novel alterations associated with pregnancy disease, Sci Rep-Uk 7 (2017) 4144.

[15] R.M. Lewis, Volume electron microscopy reveals placental ultrastructure in 3D, Placenta 141 (2023) 78–83.

[16] K. De Clercq, E. Persoons, T. Napso, C. Luyten, T.N. Parac-Vogt, A.N. Sferruzzi-Perri, G. Kerckhofs, J. Vriens, High-resolution contrast-enhanced microCT reveals the true three-dimensional morphology of the murine placenta, P Natl Acad Sci USA 116 (28) (2019) 13927–13936.

[17] W.M. Tun, G. Poologasundarampillai, H. Bischof, G. Nye, O.N.F. King, M. Basham, Y. Tokudome, R.M. Lewis, E.D. Johnstone, P. Brownbill, M. Darrow, I. L. Chernyavsky, A massively multi-scale approach to characterizing tissue architecture by synchrotron micro-CT applied to the human placenta, J. R. Soc. Interface 18 (179) (2021) 20210140.

[18] D. Laundon, B.G. Sengers, J. Thompson, S.E. Harris, O. Beasley, P.J. Basford, O. L. Katsamenis, P. Goggin, E. Derisoud, D. Fanelli, C. Bocci, F. Camillo, J. Shotton, G. Constable-Dakeyne, N.J. Gostling, P. Chavatte-Palmer, R.M. Lewis, Convergently evolved placental villi show multiscale structural adaptations to differential placental invasiveness, Biol. Lett. 20 (3) (2024) 20240016.

[19] I. Belevich, M. Joensuu, D. Kumar, H. Vihinen, E. Jokitalo, Microscopy image browser: a platform for segmentation and analysis of multidimensional datasets, PLoS Biol. 14 (1) (2016).

[20] D. Laundon, O.L. Katsamenis, J. Thompson, P. Goggin, D.S. Chatelet, P. Chavatte-Palmer, N.J. Gostling, R.M. Lewis, Correlative multiscale microCT-SBF-SEM imaging of resin-embedded tissue, Methods Cell Biol. (2023) 241–267. Academic Press.

[21] I.C. Simcock, S.C. Shelmerdine, J.C. Hutchinson, N.J. Sebire, O.J. Arthurs, Human fetal whole-body postmortem microfocus computed tomographic imaging, Nat. Protoc. 16 (5) (2021) 2594–2614.

[22] O.L. Katsamenis, P.J. Basford, S.K. Robinson, XRH-processing-toolbox, zenodo.org (2023).

[23] I. Belevich, E. Jokitalo, DeepMIB: user-friendly and open-source software for training of deep learning network for biological image segmentation, PLoS Comput. Biol. 17 (3) (2021).